J Solid State Electrochem (2007) 11: 303–309
DOI 10.1007/s10008-006-0108-0

ORIGINAL PAPER

Toshiyuki Abe · Keiji Nagai · Takeshi Matsukawa · Akio Tajiri · Takayoshi Norimatsu

Photoelectrode characteristics of an organic bilayer in water phase containing a redox molecule

Received: 21 September 2005 / Accepted: 7 February 2006 / Published online: 11 April 2006

Abstract We have recently reported that the organic bilayer of 3,4,9,10-perylenetetracarboxyl-bisbenzimidazole (PTCBI, n-type semiconductor) and 29H,31H-phthalocyanine (H_2Pc, p-type semiconductor), which is a part of a photovoltaic cell, acts as a photoanode in the water phase (Abe et al., ChemPhysChem 5:716, [2004]); in that case, the generation of the photocurrent involving an irreversible thiol oxidation at the H_2Pc/water interface took place to be coupled with hole conduction through the H_2Pc layer, based on the photophysical character of the bilayer. In the present work, the photoelectrode characteristics of the bilayer were investigated in the water phase containing a redox molecule $\left(Fe^{III/II}(CN)_6^{3-/4-}\right)$, where the photo-induced oxidation and reduction for the $Fe^{III/II}(CN)_6^{3-/4-}$ couple were found to take place at the bilayer. The photoanodic current involving the $Fe^{II}(CN)_6^{4-}$ oxidation efficiently occurred at the interface of H_2Pc/water, similar to the previous example. In the view of the voltammograms obtained, it was noted that there are pin-holes in the H_2Pc layer of the bilayer, leading to a cathodic reaction with $Fe^{III}(CN)_6^{3-}$ at the PTCBI surface especially in the dark; that is, the band bending at the PTCBI/water interface can essentially be reduced by applying a negative potential [e.g., $< \sim 0$ V (vs Ag/AgCl)] to the PTCBI, when the cathodic reaction may take place through the conduction band of the PTCBI. Moreover, under that applied potential condition of irradiation, the photogenerated electron carrier part can move to the PTCBI surface, thus enhancing the reduction of $Fe^{III}(CN)_6^{3-}$.

Keywords Photoelectrochemistry · Photoelectrode · Organic semiconductor

T. Abe (✉) · T. Matsukawa · A. Tajiri
Faculty of Science and Technology,
Hirosaki University,
3 Bunkyo-cho,
Hirosaki 036-8561, Japan
e-mail: tabe@cc.hirosaki-u.ac.jp
Fax: +81-172-393580

K. Nagai · T. Norimatsu
Institute of Laser Engineering (ILE),
Osaka University,
2-6 Yamada-oka,
Suita 565-0871, Japan

Introduction

Photoelectrochemistry is a promising method to investigate and establish a photoenergy conversion system. Molecule-based photoelectrodes are attracting much attention in terms of basic science as well as for practical application, with which highly ordered molecule-based photoelectrodes of self-assembly monolayers (SAM) [1] and Langmuir–Blodgett (LB) films [2] are now typical examples. Among the conventional molecule-based photoelectrodes, an organic bilayer of phthalocyanine and perylene derivative has been known to act as a photovoltaic cell (dry type), which involves an efficient visible light absorption and charge separation [3–6]. However, there has so far been almost no example that such a photovoltaic material of the multi-layered structure is applied to a photoelectrode especially in liquid phase.

We have recently reported that the organic bilayer, composed of 3,4,9,10-perylenetetracarboxyl-bisbenzimidazole (denoted as PTCBI, Fig. 1) and 29H,31H-phthalocyanine (denoted as H_2Pc, Fig. 1), works as a photoanode in the water phase, where an oxidation reaction is induced at the H_2Pc/water interface [7]; in details, the generation of the photoanodic current due to thiol ($-S^-$) oxidation into disulfide (–S–S–) took place to be coupled with hole conduction through the H_2Pc layer, based on the photophysical character of the bilayer. Moreover, the organic bilayer was also found to be a photoelectrode responsive to wide visible light energy of <750 nm. In the present work, the photoelectrode characteristics of the PTCBI/H_2Pc bilayer were investigated by introducing a

redox molecule $\left(Fe^{III/II}(CN)_6^{3-/4-}\right)$ into water phase (Fig. 1). As a typical result, it was noted that the photo-induced reactions for $Fe^{III/II}(CN)_6^{3-/4-}$ couple occur at the bilayer, which is different from our previous example with the irreversible thiol oxidation. The photoelectrode characteristics leading to the photoanodic and photocathodic responses are discussed in terms of voltammograms as well as action spectra for photocurrent.

Experimental

PTCBI was prepared and purified by a previous method [8]. H_2Pc was purchased from ACROS ORGANICS and purified by sublimation in a vessel thermostated at 440 °C before use (i.e., thermal control was conducted for the outside of the vessel). $K_3Fe^{III}(CN)_6$, $K_4Fe^{II}(CN)_6$, 2-mercaptoethanol, and KOH were of the purest grade from Kanto Chemical and used as received. The indium-tin-oxide (ITO)-coated glass plate (sheet resistance, 13 Ω cm^{-2}; transmittance, 85%; ITO thickness, 110 nm) was from Nippon Sheet Glass.

The photoelectrode device of PTCBI/H_2Pc was prepared by vapor deposition (degree of the vacuum, $<1.0\times10^{-3}$ Pa; deposition speed, 0.03 nm s^{-1}) and consisted of PTCBI coated on an ITO plate and H_2Pc coated on top of the PTCBI (denoted as ITO/PTCBI/H_2Pc). During vapor deposition, the temperature at the ITO plate was not controlled. Absorption spectral measurement was conducted using a Hitachi U-2010 spectrophotometer. The resulting absorption spectra of both PTCBI and H_2Pc were identical to those reported earlier [4], and their absorption coefficients indicated the thickness of the film employed (cf., the aggregation structure of the H_2Pc single layer can also be identified from the absorption spectrum; that is, the polymorph of H_2Pc was assignable to the alpha-phase, which is also supported by an earlier study [9]). As the additivity of the absorption coefficients is considered to be held on the visible light absorption spectrum of the bilayer, the two unknown parameters of each thickness were estimated by solving simultaneous equations on absorbance at two distinct wavelengths.

An electrochemical cell was equipped with the modified ITO working, a spiral Pt counter, and an Ag/AgCl (in saturated KCl electrolyte) reference electrode. The photoelectrochemical study was conducted using a potentiostat (Hokuto Denko, HA-301) with a function generator (Hokuto Denko, HB-104), a coulomb meter (Hokuto Denko, HF-201), and an X–Y recorder (GRAPHTEC, WX-4000) under illumination. A 150-W halogen lamp (light intensity, 70 mW cm^{-2}) was used as a light source under typical conditions. The entire photoelectrochemical study was run in an alkaline water containing a known concentration of the redox molecule ($K_4Fe^{II}(CN)_6$ or $K_3Fe^{III}(CN)_6$) in an Ar atmosphere (cf., a concentrated KOH solution was used to be adjusted to pH 10). The electrolyte solution of thiol was also prepared according to the above method. In measuring action spectrum, a halogen lamp (300 W) was used as a light source in combination with a monochromator (SOMA OPTICS, S-10). The light intensity was measured using a power meter (type 2A from OPHIR JAPAN). In the present study, the effect of the reflection of the incident light from the glass surface was not considered (i.e., the light intensity was not corrected).

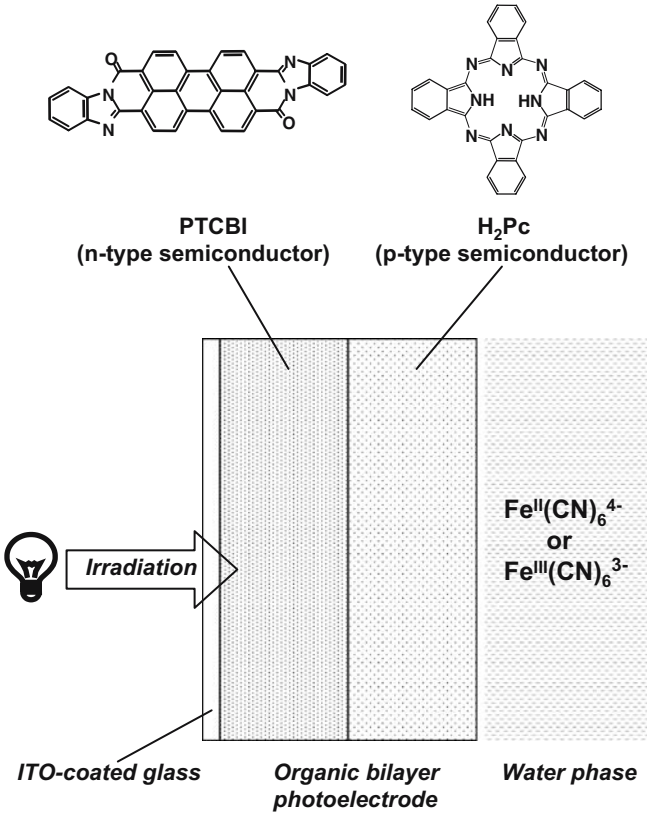

Fig. 1 Chemical structures of perylene derivative (*PTCBI*) and phthalocyanine (*H_2Pc*), and a schematic illustration for photo-induced reaction at PTCBI/H_2Pc bilayer in water phase

Results and discussion

Typical photoelectrode characteristics of PTCBI/H_2Pc bilayer

The photoelectrode characteristics of PTCBI/H_2Pc bilayer were first investigated by means of voltammetry. Figure 2 shows a typical cyclic voltammogram (CV) at ITO/PTCBI/H_2Pc in the presence of an aqueous thiol (2-mercaptoethanol), compared with that at ITO/PTCBI (single layer). The photoanodic current due to the thiol oxidation can be confirmed efficiently occurring at the interface of H_2Pc/water (I in Fig. 2) rather than at that of PTCBI/water (II in Fig. 2). Note that the photoelectrochemical event in I (Fig. 2) is evidently different from the ordinary photoelectrode characteristics at the p-type semiconductor/liquid interface of the Schottky junction [7]. Moreover, as for the bilayer, the photo-induced oxidation took place at the

potential less positive than the formal potential for $-S^{\cdot}/-S^{-}$ couple (~ +0.6 V vs Ag/AgCl [10]). Considering both the potential for $-S^{\cdot}/-S^{-}$ couple and the oxidative potential of H_2Pc (+0.64 V vs SCE [11]; ca. +0.69 V vs Ag/AgCl), it appears that the thiol oxidation is induced by the oxidative power photogenerated at the H_2Pc/water interface, which is coupled with hole conduction through the H_2Pc layer.

The thiol ($-S^{-}$) undergoes an irreversible oxidation into disulfide (–S–S–) via the coupling of the anion radical species ($-S^{\cdot}$) [12]. However, when measuring CV in the water phase containing a redox molecule $\left(Fe^{II}(CN)_6^{4-}\right)$ (Fig. 3a), the voltammogram noticeably differed from that in I in Fig. 2. Firstly, the CV characteristics in anodic scan are discussed. When measuring the CVs in the presence of $Fe^{II}(CN)_6^{4-}$, the photoanodic current due to the $Fe^{II}(CN)_6^{4-}$ oxidation occurred at the potentials more positive than −0.2 V (I in Fig. 3a); however, no electrochemical response was observed in the dark (II in Fig. 3a). Furthermore, a CV for $Fe^{III/II}(CN)_6^{3-/4-}$ couple was measured at a bare ITO in the dark (Fig. 3b), compared with I in Fig. 3a. Based on the difference between those CV characteristics, it evidently shows that the photoanodic current generation is induced by the oxidative power photogenerated at the bilayer.

In addition to the photoanodic response with $Fe^{II}(CN)_6^{4-}$ oxidation, a photocathodic response appeared due to the reduction of the oxidized species (i.e., $Fe^{III}(CN)_6^{3-}$). When comparing Fig. 3b with I in Fig. 3a, it was noted that the potential at which the reduction of $Fe^{III}(CN)_6^{3-}$ into $Fe^{II}(CN)_6^{4-}$ takes place is less positive at the latter than at the former. If the photocathodic response corresponds to a photocatalytic event induced on an absorption at the interface of H_2Pc/water of the Schottky junction, the cathodic reaction should take place at the potentials positive than that in the Fig. 3b [cf., the photogenerated reductive power of H_2Pc can be estimated as −1.31 V vs Ag/AgCl (*vide infra*)]; that is, the photocathodic response cannot be associated with a visible light absorption at the H_2Pc/water interface.

A control experiment was carried out to gain insights into the photoelectrode characteristics of Fig. 3a, for which irradiation was performed only in the initial scan towards the anodic direction; subsequently, the cathodic scan was

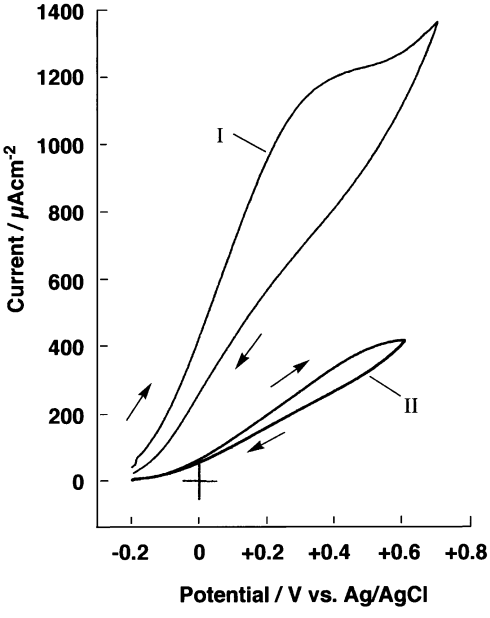

Fig. 2 CVs at both ITO/PTCBI/H_2Pc (I) and ITO/PTCBI (II) under illumination. Scan rate, 20 mV s^{-1}; thiol concentration, 1.0×10^{-2} mol dm^{-3} (pH 10); Film thickness (for bilayer), 230 nm (PTCBI)/50 nm (H_2Pc); Film thickness (for single layer), 230 nm (PTCBI)

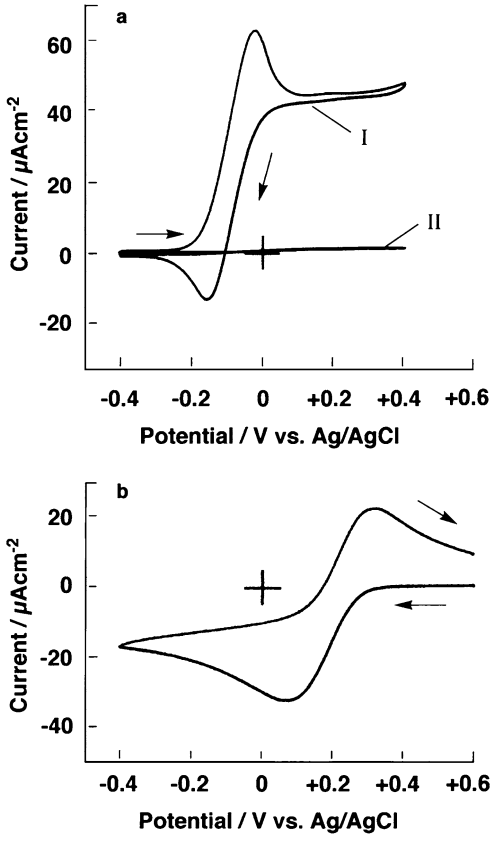

Fig. 3 (**a**) CV at ITO/PTCBI/H_2Pc under illumination (I) and dark (II). Scan rate, 5 mV s^{-1}; $K_4Fe^{II}(CN)_6$ concentration, 1.0×10^{-3} mol dm^{-3} (pH 10); Film thickness (for I and II), 200 nm (PTCBI)/70 nm (H_2Pc). (**b**) CV at a bare ITO in the dark. Scan rate, 5 mV s^{-1}; $K_3Fe^{III}(CN)_6$ concentration, 1.0×10^{-3} mol dm^{-3} (pH 10). (**c**) CV at ITO/PTCBI/H_2Pc. The CV scan was initiated towards the anodic direction under illumination, and subsequently, the cathodic scan was run by switching illumination off at +0.4 V (vs. Ag/AgCl). Scan rate, 5 mV s^{-1}; $K_4Fe^{II}(CN)_6$ concentration, 1.0×10^{-3} mol dm^{-3} (pH 10); Film thickness, 300 nm (PTCBI)/70 nm (H_2Pc). (**d**) CV at ITO/PTCBI/H_2Pc in the presence (I) and the absence (II) of $K_3Fe^{III}(CN)_6$ (in the dark). Scan rate, 5 mV s^{-1}; $K_3Fe^{III}(CN)_6$ concentration, 1.0×10^{-3} mol dm^{-3} (pH 10); Film thickness (for I and II), 350 nm (PTCBI)/70 nm (H_2Pc). (**e**) CVs at ITO/PTCBI in the dark (I) and under illumination (II) in the presence of $K_4Fe^{II}(CN)_6$. Scan rate, 5 mV s^{-1}; $K_4Fe^{II}(CN)_6$ concentration, 1.0×10^{-3} mol dm^{-3} (pH 10); Film thickness (for I and II), 200 nm (PTCBI). (**f**) CVs at ITO/PTCBI in the dark (I) and under illumination (II) in the presence of $K_3Fe^{III}(CN)_6$. Scan rate, 5 mV s^{-1}; $K_3Fe^{III}(CN)_6$ concentration, 1.0×10^{-3} mol dm^{-3} (pH 10); Film thickness (for I and II), 200 nm (PTCBI)

Fig. 3 (continued)

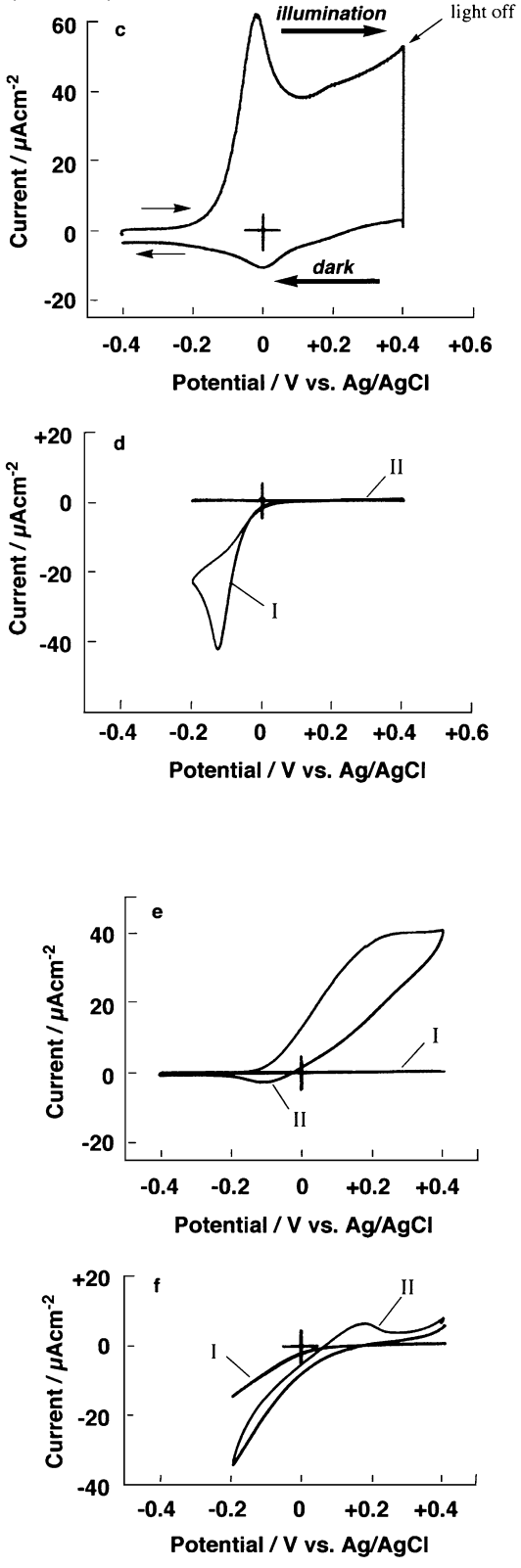

run after switching illumination off at +0.4 V (Fig. 3c). From the result of Fig. 3c, no disappearance of a similar cathodic peak to Fig. 3a can be confirmed on the voltammogram. Furthermore, CVs at the bilayer were also measured in the presence and the absence of $Fe^{III}(CN)_6^{3-}$ in the dark (Fig. 3d), where the CV scan was initiated towards the cathodic direction. In the presence of $Fe^{III}(CN)_6^{3-}$ (I in Fig. 3d), its reduction was observed to take place at the bilayer, but no electrochemical response for the reoxidation of $Fe^{II}(CN)_6^{4-}$ occurred. In the absence of $Fe^{III}(CN)_6^{3-}$ (II in Fig. 3d), there was no electrochemical response. The voltammetric results of Fig. 3c,d indicate that the $Fe^{III}(CN)_6^{3-}$ reduction is induced under electrochemical process especially in the dark.

Further control experiments were carried out using ITO/PTCBI (single layer) in the presence of $Fe^{II}(CN)_6^{4-}$ or $Fe^{III}(CN)_6^{3-}$. The CV scan, initiated from −0.4 V towards the anodic direction, was conducted in the presence of $Fe^{II}(CN)_6^{4-}$. In the dark, there was not any electrochemical response (I in Fig. 3e), while the ordinary photoanodic response at the n-type semiconductor (PTCBI)/water interface was observed under illumination (II in Fig. 3e), followed by the reduction of $Fe^{III}(CN)_6^{3-}$ in the reverse CV scan. The CVs at the ITO/PTCBI were also measured in the presence of $Fe^{III}(CN)_6^{3-}$ (cf., the potential scan was initiated from +0.4 V towards the cathodic direction), from which it was noted that the cathodic features in the dark (I in Fig. 3f) are consistent with that at ITO/PTCBI/H_2Pc (see Fig. 3d). Moreover, the cathodic reaction involving the $Fe^{III}(CN)_6^{3-}$ reduction was efficiently enhanced under illumination (II in Fig. 3f). In summary, from those voltammetric aspects, it should be realized that there are pin-holes in the H_2Pc layer of the bilayer; that is, the PTCBI has direct contact with $Fe^{III}(CN)_6^{3-}$. Comparing I in Fig. 3a with I in Fig. 3e, it evidently shows that the photoanodic reaction is induced at the H_2Pc/water interface rather than at the PTCBI/water interface (cf., the same thickness as the PTCBI layer was employed in the bilayer as well as in the single layer and, in each case, the irradiation was conducted from the side of ITO/PTCBI interface); however, the cathodic reaction involving the $Fe^{III}(CN)_6^{3-}$ reduction occurs at the PTCBI surface in the dark. The cathodic reaction may be induced with an overlap of the energy level between the conduction band (PTCBI) and $Fe^{III/II}(CN)_6^{3-/4-}$ [cf., ~0 V (vs Ag/AgCl) for PTCBI (*vide infra*), and ~+0.20 V (vs Ag/AgCl) for $Fe^{III/II}(CN)_6^{3-/4-}$ (cf., Fig. 3b)]; that is, the band bending at the PTCBI/water interface can essentially be reduced by applying a negative potential to the PTCBI, when the cathodic reaction may take place through the conduction band of the PTCBI. Moreover, under that applied potential condition of irradiation, the photogenerated electron carrier part can move to the PTCBI surface, thus enhancing the cathodic reaction. Similar to the cathodic reaction at the n-type semiconductor, the anodic reaction (dark reaction) at p-type semiconductor (single layer of zinc phthalocyanine) has also been reported [13]. The details for the mechanism on the present photocurrent generation are discussed later.

Figure 4 shows typical current changes at the ITO/PTCBI/H_2Pc soaked in an aqueous $Fe^{II}(CN)_6^{4-}$ (a) or $Fe^{III}(CN)_6^{3-}$ (b), which is induced by switching illumination on and off. The steady photocurrent generation was confirmed under both photoanodic (a) and photocathodic (b) conditions.

Measurement of action spectrum for photocurrent

The action spectrum for photocurrent was measured to understand the origin of the photocurrent generated at the ITO/PTCBI/H_2Pc. The incident photon-to-current conversion efficiency (IPCE) was calculated by the following equation (Eq. 1),

$$IPCE(\%) = \left([I/e]/[W/\varepsilon]\right) \times 100 \quad (1)$$

where I (A cm^{-2}) is the photocurrent density, e (C) is the elementary electric charge, W (W cm^{-2}) is the light intensity, and ε is the photon energy.

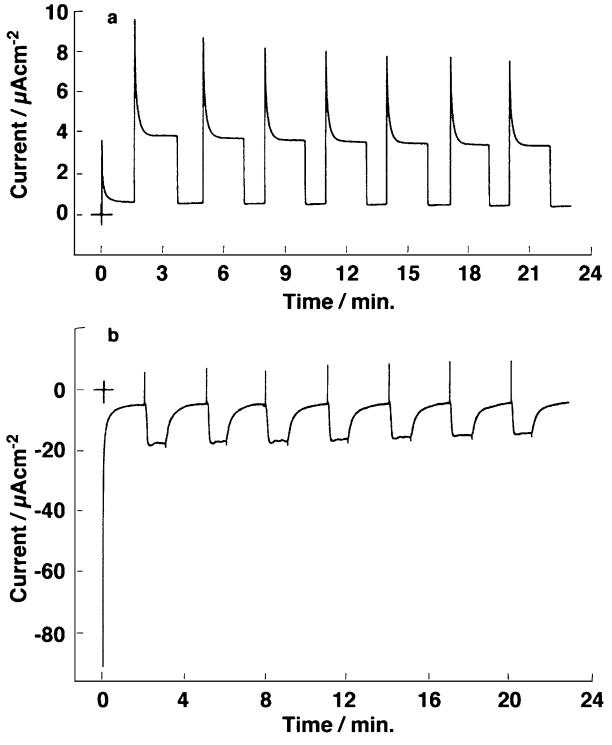

Fig. 4 Typical changes of both anodic (**a**) and cathodic (**b**) currents induced by on and off of illumination at ITO/PTCBI/H_2Pc. Applied potential, +0.4 V (vs. Ag/AgCl) for (**a**) and −0.15 V (vs. Ag/AgCl) for (**b**); Concentrations of $K_4Fe^{II}(CN)_6$ (for **a**) and $K_3Fe^{III}(CN)_6$ (for **b**), 1.0×10^{-3} mol dm^{-3} (pH 10); Film thickness (for **a**), 420 nm (PTCBI)/140 nm (H_2Pc); Film thickness (for **b**), 360 nm (PTCBI)/150 nm (H_2Pc)

Origin of photoanodic current generation

The action spectra for the photoanodic current were measured in terms of irradiation direction on incident light (Fig. 5). The monochromatic light irradiation was first conducted from the PTCBI side (I in Fig. 5a), in which the photocurrent was found to be generated over the wavelength employed. It should also be noted that, in spite of having no absorption of H_2Pc at around 500 nm (cf., transmittance spectrum of H_2Pc single layer in Fig. 5a), the photocurrent is generated. The photoelectrochemical event involving the photoanodic current generation was explicitly realized by irradiating the monochromatic light from the H_2Pc side (II in Fig. 5a), on which the resulting action spectrum was found to agree with the transmittance spectrum of H_2Pc. Therefore, from the results of Fig. 5, it can be concluded that the present photoanodic current is induced on a wide visible light absorption by only the PTCBI; that is, the action spectrum was not in agreement with the absorption spectrum of the PTCBI/H_2Pc employed (Fig. 5b), showing that the photoanodic current generation cannot be induced on the visible light absorption over the whole layer of PTCBI/H_2Pc. The present action spectral characteristics are in accord with our previous case where an absorption in the PTCBI bulk was effective for a photocurrent generation [7]. However, the resulting action spectral characteristics are different from those of the conventional organic photovoltaic cells where it has been characterized that an absorption by both layers contributes to a photocurrent generation [3–6, 14–16]. This might be ascribed to slower photoelectrode kinetics at the present solid/liquid interface than the hole transport at a phthalocyanine/ITO interface in the dry cells.

In addition, when comparing II with I, the IPCE values are relatively higher in the former than in the latter, especially in shorter wavelength than 550 nm where the absorption of H_2Pc is absent or weak. When considering the absorbance of the whole PTCBI layer (for film II) at 475 nm, the quantum yield was estimated to be ~9%, which indicates a high efficiency on the photoenergy conversion. This could suggest that the absorption of PTCBI located near the PTCBI/H_2Pc interface leads to the more efficient carrier generation.

Origin of photocathodic current generation

The action spectra for the photocathodic current were also measured by employing the same procedure as in Fig. 5a, and the results are shown in Fig. 6. The dependencies of the resulting action spectra on irradiation direction were similar to Fig. 5a. As also supported by the voltammetric characteristics in Fig. 3, those action spectra showed that an absorption of the single-layered PTCBI induces the photocurrent generation.

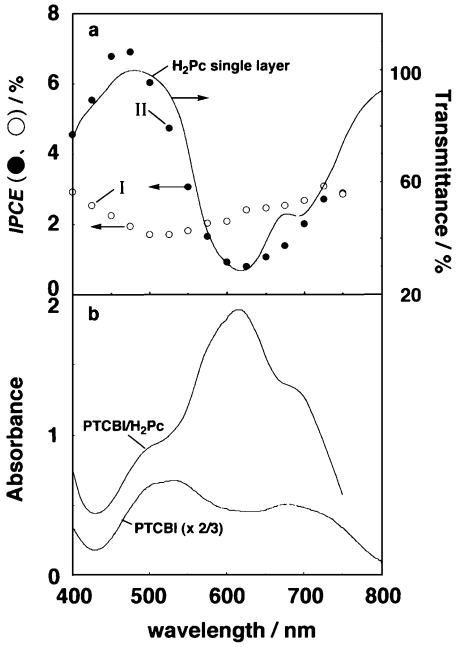

Fig. 5 (**a**) Action spectra for photoanodic current generated at ITO/PTCBI/H_2Pc (○ for I, ● for II), and transmittance spectrum of H_2Pc single layer (solid line). Irradiation with monochromatic light; ITO/PTCBI side for I and H_2Pc/water side for II. Applied potential, +0.3 V (vs. Ag/AgCl); $K_4Fe^{II}(CN)_6$ concentration, 1.0×10^{-3} mol dm^{-3} (pH 10); Film thickness for bilayer (I and II), 300 nm (PTCBI)/70 nm (H_2Pc); Film thickness for H_2Pc single layer (transmittance spectrum), 50 nm. (**b**) Absorption spectra of PTCBI (300 nm)/H_2Pc (70 nm), and PTCBI single layer (320 nm)

Mechanism on photoanodic current generation

The energy levels for ITO [17], PTCBI [17, 18], H_2Pc [19], $-S^{\cdot-}/-S^{-}$, and $Fe^{III}(CN)_6^{3-}\big/Fe^{II}(CN)_6^{4-}$ couple are summarized in Fig. 7. As for the quenching of photoluminescence of PTCBI [20], it has been reported that the quenching efficiently takes place in contact with the H_2Pc layer; in other words, it showed that charge separation is possible only on the absorption by PTCBI (Eq. 2),

$$PTCBI^{*} - H_2Pc \rightarrow PTCBI^{-} - H_2Pc^{+} \qquad (2)$$

where PTCBI* is exciton of PTCBI. In addition, the laser ablation properties of the bilayer exhibited uniform ablation trace due to free electrons in PTCBI layer and efficient absorption of high power laser of 1.06 μm, indicating accumulation of $PTCBI^{-}$ by only coating with H_2Pc and light irradiation [21]. After the charge separation, the photogenerated carriers of $PTCBI^{-}$ and H_2Pc^{+} can migrate in each layer. The photoanodic current cannot originate from the photoconduction of only the H_2Pc single layer, because the action spectrum of Fig. 5 suggested no contribution from the absorption of H_2Pc. However, according to Eq. 2, the conduction in the H_2Pc layer of PTCBI/H_2Pc can be explained by the photogeneration of H_2Pc^{+} acting as hole carrier; that is, the photogenerated and migrated H_2Pc^{+} induces the photoanodic current generation at the H_2Pc/water interface (Eq. 3).

$$H_2Pc^{+} + Fe^{II}(CN)_6^{4-}(or - S^{-}) \rightarrow H_2Pc + Fe^{III}(CN)_6^{3-}(or - S^{\bullet-}) \qquad (3)$$

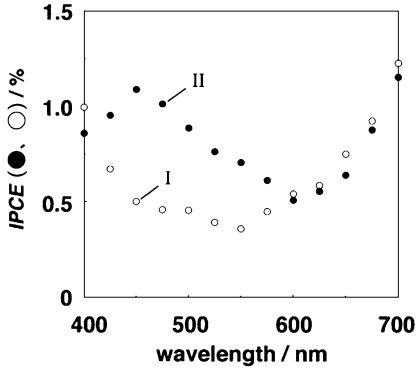

Fig. 6 Action spectra for photocathodic current generated at ITO/PTCBI/H_2Pc (○ for I, ● for II). Irradiation with monochromatic light; PTCBI side for I and H_2Pc side for II; Applied potential, −0.1 V (vs. Ag/AgCl); $K_3Fe^{III}(CN)_6$ concentration, 1.0×10^{-3} mol dm^{-3} (pH 10); Film thickness, 300 nm (PTCBI)/70 nm (H_2Pc). Absorption spectrum of PTCBI/H_2Pc as well as transmittance spectrum of H_2Pc should refer to Fig. 5

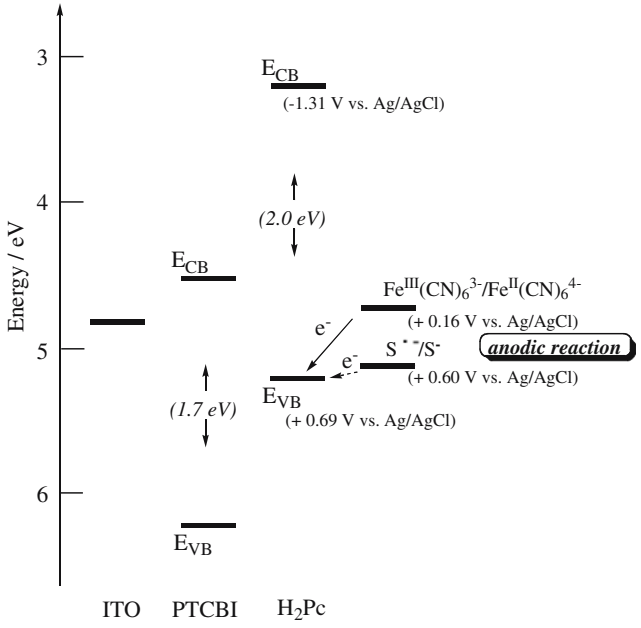

Fig. 7 Schematic diagram on energy levels for ITO, PTCBI, H_2Pc, $S^{\cdot-}/S^{-}$ and $Fe^{III}(CN)_6^{3-}/Fe^{II}(CN)_6^{4-}$ couple. Energy levels for valence band and conduction band are denoted as E_{VB} and E_{CB}, respectively

Acknowledgement This work was partially supported by a Grant-in-Aid for Scientific Research (No. 15750110) from Ministry of Education, Culture, Sports, Science and Technology, Japan (T. A.).

References

1. Imahori H, Hosomizu K, Mori Y, Sato T, Ahn T-K, Kim S-K, Kim D, Nishimura Y, Yamazaki I, Ishii H, Hotta H, Matano Y (2004) J Phys Chem B 108:5018
2. Yang S, Fan L, Yang S (2004) J Phys Chem B 108:4394
3. Tang CW (1986) Appl Phys Lett 48:183
4. Morikawa T, Adachi C, Tsutsui T, Saito S (1990) Nippon Kagaku Kaishi 962
5. Hiramoto M, Fukusumi H, Yokoyama M (1992) Appl Phys Lett 61:2580
6. Wöhrle D, Kreienhoop L, Schnurpfeil G, Elbe J, Tennigkeit B, Hiller S, Schlettwein D (1995) J Mater Chem 5:1819
7. Abe T, Nagai K, Kaneko M, Okubo T, Sekimoto K, Tajiri A, Norimatsu T (2004) ChemPhysChem 5:716
8. Maki T, Hashimoto H (1952) Bull Chem Soc Jpn 25:411
9. Sharp JH, Lardon M (1968) J Phys Chem 72:3230
10. Surdhar S, Armstrong DA (1986) J Phys Chem 90:5915
11. Lever ABP, Milaeva ER, Speier G (1993) The redox chemistry of metallo-phthalocyanines in solution. In: Leznoff CC, Lever ABP (eds), Phthalocyanines, vol. 3. VCH, New York, pp 2–69
12. Zagal JH, Gulppi MA, Caro CA, Cárdenas-Jirón GI (1999) Electrochem Commun 1:389
13. Schlettwein D, Kaneko M, Yamada A, Wöhrle D, Jaeger NI (1991) J Phys Chem 95:1748
14. Hill IG, Kahn A (1999) J Appl Phys 86:2116
15. Stübinger T, Brütting W (2001) J Appl Phys 90:3632
16. Hiromitsu I, Murakami Y, Ito T (2003) J Appl Phys 94:2434
17. Yakimov A, Forrest SR (2002) Appl Phys Lett 80:1667
18. Hill IG, Schwartz J, Kahn A (2000) Org Electron 1:5
19. Loutfy RO, Cheng YC (1980) J Chem Phys 73:2902
20. Nagai K, Fujimoto Y, Shiroishi H, Kaneko M, Norimatsu T, Yamanaka T (2001) Chem Lett 354
21. Nagai K, Yoshida H, Norimatsu T, Miyanaga N, Izawa Y, Yamanaka T (2002) Appl Surf Sci 197:808